Colloid and Interface Science Communications 42 (2021) 100389

Contents lists available at ScienceDirect

Colloid and Interface Science Communications

journal homepage: www.elsevier.com/locate/colcom

Ionic strength and zeta potential effects on colloid transport and retention processes

Mandana Samari-Kermani [a,b], Saeed Jafari [a,*], Mohammad Rahnama [a], Amir Raoof [b]

[a] Department of Mechanical Engineering, Shahid Bahonar University of Kerman, Kerman, Iran
[b] Department of Earth Sciences, Utrecht University, Utrecht, the Netherlands

ARTICLE INFO

Keywords:
Colloid transport
Pore scale
Aggregation
Ionic strength
Zeta potential
Lattice Boltzmann method
Smoothed profile method

ABSTRACT

In this study, a fully coupled pore scale model was developed with the aim of exploring the effects of ionic strength and zeta potential on colloids transport under favourable and unfavourable conditions. The Lattice Boltzmann-Smoothed Profile method was used to simulate particle-particle and particle-fluid interactions without a need for assumptions of dilute suspension and clean bed filtration. Simulation using a wide range of parameters have shown creation, and breakup of agglomerates. Results are used to obtain time-averaged behaviour of transport properties, such as pore void fraction, conductivity, and surface coverage. We have found that in comparison with zeta potential, increasing ionic strength had a greater impact on particles behaviour. A raise in ionic strength caused a decrease in pore void fraction and its conductivity and an increase in aggregates connectivity.

1. Introduction

A fundamental understanding of colloid transport and retention is critical for human health and environmental issues concerning behaviour of microparticles, viruses and bacteria [1–3]. While several studies have used field and column experiments to explore the controlling mechanisms of colloid transport [4–7], some others have utilized modelling and numerical simulations to investigate particles transport and retention mechanisms [8–12]. Studies have shown that particle retention in porous media depends on the number of inter particle collisions and the available fraction of surface area for attachment. While this fraction is larger for increasing ionic strengths (IS) of the solution, collector size, physical and chemical heterogeneities, it is lower for larger pore velocities, particle sizes, magnitude and ratio of colloid and collector surface potentials [9,13–15]. Physical and chemical heterogeneities may significantly affect colloid retention by changing the effective interaction energy profiles. It has been shown that the extent of energy barrier is decreased for larger IS values, chemical heterogeneity, and temperature particularly for non-smooth surfaces [7,8,16,17].

Transport and retention of colloids become more complex when agglomerates are formed. Aggregation and fragmentation change size and structure of aggregates as well as the concentration of colloids suspended within the solution phase [12,18–20]. Flow velocity, solution pH, IS, colloids shape and solid volume fraction are among parameters that can affect the size and structure of aggregates [20–24]. Larger volumetric fraction of colloids, and pH values close to the isoelectric point result in transformation of chain-like aggregates into more complex and compact net-like structures [21].

When porous media is saturated, colloid filtration theory, CFT, is used to predict particle deposition [25]. This theory assumes dilute suspensions in which particles are so far apart that they do not interact with each other. The assumption of free-floating particles in a 3D pore space may not be valid in natural applications. CFT neglects the effect of secondary energy minimum, and assumes adsorption under clean bed filtration. Additionally, CFT considers homogeneous and large surface area where the deposited particles do not lower the attachment capacity. As a result of these assumptions, several studies have reported breakdown of this theory [26,27] and progress is being made to understand the influencing parameters using mechanistic exploration of particles transport and their adsorptive behaviour.

Kermani et al. (2020) applied direct pore scale simulations to investigate the impact of hydrodynamic forces, colloid size, and pore structure on transport and retention of colloids [12]. They have developed coupled formulas representing fluid flow and particles motion using lattice Boltzmann and smoothed profile methods. In this study, we use the numerical method developed in Kermani et al. (2020) to

* Corresponding author.
E-mail address: jafari@uk.ac.ir (S. Jafari).

https://doi.org/10.1016/j.colcom.2021.100389
Received 27 December 2020; Received in revised form 9 February 2021; Accepted 22 February 2021
Available online 13 March 2021

mechanistically explore the effects of ionic strength and zeta potential on transport of particles. This helps to study how changes of these parameters affect aggregation, and retention mechanisms with no need for simplifying assumptions like clean bed filtration or dilute suspension. The complete set of simulations are analysed to provide time-averaged values (or its corresponding dimensionless number, Pore Volume) for several key parameters including pore conductivity, void fraction, surface coverage, and particles coordination number. The time-averaged graphs are used to provide dominant properties for different magnitudes of ionic strength and zeta potential when a stable behaviour is reached. These observations provide an upscaled view of colloid transport which is needed to provide findings of pore scale studies to larger scales. In some cases, the complex interplay between transport and sorption processes may cause very dynamic and transient variations in colloid behaviour which are explained using the underlying time-dependent changes of the system. Time-dependent graphs help to reveal interactions of the incoming particles with those inside the pore and their contribution to development of the effects such as the shadow zone. The observed behaviour provide basis for more reliable predictions under realistic situations and for larger scale models which use effective parameters and do not consider time scales associated with detailed pore scale processes.

2. Methodology

To simulate the particulate flow, a coupled, two-dimensional smoothed profile-lattice Boltzmann method is selected that can efficiently handle particle-fluid interactions [28,29]. The Smoothed profile method (SPM) is used to simulate particle dispersions and the two-way hydrodynamic interactions [30].

Simulations are performed in two steps. First, a steady state flow is simulated such that the desired average pore velocity, U, is obtained based on the applied boundary conditions. Second, the particle injection starts. During this step, fluid velocity field, $\boldsymbol{u}(\boldsymbol{x},t)$, is dynamically recalculated at each time step using the coupled formulation with SPM.

We have considered the following assumptions in our simulations:

- Particles and pore surfaces are physically homogeneous, i.e. there is no roughness on the surfaces.
- Particles and pore surfaces are chemically homogeneous and uniformly charged.
- Particle-pore surface interactions are calculated using sphere-plate equations.
- Molecular diffusion impacts transport of particles with sizes smaller than 1 μm [25,39]. Therefore, the effect of molecular diffusion is neglected in this study which considers particle sizes of 3, 5 and 10 μm.

We should mention that physical, chemical, and charge homogeneity of the pore surfaces are the initial conditions. However, these conditions change during the simulations due to particles retention and their accumulation on the surface.

3. Mathematical modelling

3.1. Lattice Boltzmann method

The discretized form of Boltzmann equation with single relaxation time, an external force term, $\boldsymbol{F}$, and BGK (Bhatnagar-Gross-Krook) collision operator is shown in Eq. (1) [31–33].

$$f_\alpha(\boldsymbol{x}+\boldsymbol{e_\alpha}\Delta t, t+\Delta t) - f_\alpha(\boldsymbol{x},t) = -\frac{1}{\tau}\left[f_\alpha(\boldsymbol{x},t) - f_\alpha^{eq}(\boldsymbol{x},t)\right] - 3\omega_\alpha \rho \boldsymbol{e_\alpha}.\frac{\boldsymbol{F}}{c^2} \tag{1}$$

$$f_\alpha^{eq} = \rho\omega_\alpha\left[1 + 3\frac{\boldsymbol{e_\alpha}.\boldsymbol{u}}{c^2} + \frac{9}{2}\frac{(\boldsymbol{e_\alpha}.\boldsymbol{u})^2}{c^4} - \frac{3}{2}\frac{\boldsymbol{u}.\boldsymbol{u}}{c^2}\right] \tag{2}$$

where $\boldsymbol{x}$, t, and c are lattice position, time, and speed, respectively. f is the distribution function, which describes the behaviour and motion of fluid particles in space. Distribution functions can relax toward their equilibrium values, f^{eq}, and can be transported along predefined directions, α.

$$\omega_\alpha = \begin{cases} 4/9 & \alpha = 0 \\ 1/9 & \alpha = 1,2,3,4 \\ 1/36 & \alpha = 5,6,7,8 \end{cases} \text{ and } \boldsymbol{e_\alpha}$$

$$= \begin{cases} (0,0) & \alpha = 0 \\ (1,0),(0,1),(-1,0),(0,-1) & \alpha = 1,2,3,4 \\ (1,1),(-1,1),(-1,-1),(1,-1) & \alpha = 5,6,7,8. \end{cases}$$

are the weight coefficients and discrete velocity vectors in α directions in the D2Q9 lattice structure used in this study.

Macroscopic quantities can be calculated in terms of distribution functions as:

$$\rho(\boldsymbol{x},t) = \sum_{\alpha=0}^{8} f_\alpha(\boldsymbol{x},t) \tag{3}$$

$$\rho(\boldsymbol{x},t)\boldsymbol{u}(\boldsymbol{x},t) = \sum_{\alpha=0}^{8} \boldsymbol{e_\alpha} f_\alpha(\boldsymbol{x},t) \tag{4}$$

$$p(\boldsymbol{x},t) = (\rho(\boldsymbol{x},t))/3 \tag{5}$$

3.2. Smoothed profile method

SPM represents each particle by a smooth profile, φ_P, which equals unity in the particle domain, zero in the fluid domain, and changes smoothly between one and zero in the fluid-solid interfacial region, ξ [28,30]. Eq. (6) shows the profile for round shape particles used in this study.

$$\varphi_P(\boldsymbol{x}t) = s(R_P - |\boldsymbol{x} - \boldsymbol{R}_P(t)|)$$

$$R_P - |\boldsymbol{x} - \boldsymbol{R}_P(t)| = L_P$$

$$s(L_P) = \begin{cases} 0 & L_P < -\xi/2 \\ \frac{1}{2}\left(sin\left(\frac{\pi L_P}{\xi}\right) + 1\right) & |L_P| \le \xi/2 \\ 1 & L_P > \xi/2 \end{cases} \tag{6}$$

where R_P, and $\boldsymbol{R_P}$ are the radius, and the position vector of each particle, respectively. Eqs. (7) and (8) show the total profile function, $\varphi(\boldsymbol{x},t)$, and the particle velocity field, $\boldsymbol{u_P}(\boldsymbol{x},t)$, obtained from rigid motions of all N_P particles at time t and position $\boldsymbol{x}$.

$$\varphi(\boldsymbol{x},t) = \sum_{P=1}^{N_P} \varphi_P(\boldsymbol{x},t) \tag{7}$$

$$\varphi(\boldsymbol{x},t)\,\boldsymbol{u_P}(\boldsymbol{x},t) = \sum_{P=1}^{N_P} \varphi_P(\boldsymbol{x},t)\left[\boldsymbol{U}_{C_p}(t) + \boldsymbol{\omega}_P \times \{\boldsymbol{x} - \boldsymbol{R}_P(t)\}\right] \tag{8}$$

$$f_H = -\varphi(\boldsymbol{x},t) f_P(\boldsymbol{x},t) = -\varphi(\boldsymbol{x},t)(\boldsymbol{u_P}(\boldsymbol{x},t) - \boldsymbol{u}(\boldsymbol{x},t)) \tag{9}$$

where $\boldsymbol{U}_{Cp}$ and $\boldsymbol{\omega}_P$ are translational and angular velocities of particles, respectively. To ensure no-slip boundary condition, SPM updates the velocity of each virtual fluid node covered by solid particles by considering a body force, f_H.where $\boldsymbol{u}(\boldsymbol{x},t)$ is the fluid velocity field, and $-\varphi(\boldsymbol{x},t)f_P(\boldsymbol{x},t)$ represents the fluid-solid interaction force acting on virtual fluid nodes inside the particles. The integrated hydrodynamic force, $\boldsymbol{F}_P^H$, and torque, $\boldsymbol{T}_P^H$, on each individual particle can be obtained using Eqs. (10) and (11).

$$\boldsymbol{F}_P^H = \int_{\forall_p} \rho\varphi(\boldsymbol{x},t)\left(\boldsymbol{u}(\boldsymbol{x},t) - \boldsymbol{u}_p(\boldsymbol{x},t)\right) d\forall_p \tag{10}$$

$$\boldsymbol{T}_P^H = \int_{\forall_p} (\boldsymbol{x} - \boldsymbol{R}_P) \times \rho\varphi(\boldsymbol{x},t)\left(\boldsymbol{u}(\boldsymbol{x},t) - \boldsymbol{u}_p(\boldsymbol{x},t)\right) d\forall_p \tag{11}$$

3.3. Coupling SPM with LBM

Luo suggested that in LBM the external force term, $\boldsymbol{F}$, can be introduced into the collision term as $-3\omega_\alpha \rho \boldsymbol{e_\alpha}.\frac{\boldsymbol{F}}{c^2}$ shown in Eq. (1) [32]. In SPM, particles rigidity is imposed to each fluid node covered by solid particles using a smooth body force, f_H, calculated in Eq. (9). To consider the mutual effects of particles and flow streamlines, f_H replaces the external force vector $\boldsymbol{F}$ in each time step.

3.4. DLVO interactions

Particle-particle as well as particle-surface interaction energies are calculated using DLVO (Derjaguin-Landau-Verwey-Overbeek) theory which considers the combined effect of van der Waals and electrostatic double layer interactions [34–36]. Using DLVO theory, under attractive double layer interactions (favourable conditions), there is no energy barrier to act against deposition of particles at the primary energy minimum (PEM). However, under repulsive double layer interactions (unfavourable conditions), irreversibility of deposition at the surface PEM depends on height of the energy barrier as well as depth of the secondary energy minimum (SEM). As the energy difference between the barrier and the secondary minimum increases, fewer particles will have sufficient kinetic energy to pass the barrier and deposit at the PEM [37]. As shown in Supplementary information Fig. S1, the energy barrier increases in height with decreasing IS, increasing zeta potential, and particle size. Alternatively, the SEM depth increases with increasing IS, and particle size, but decreasing zeta potential.

In the present simulations, all particles are similarly charged and aggregation condition is unfavourable. Particles make agglomerates through SEM interactions (these particles are indicated by orange colour in the figures of this study). Retention at the pore surface can be favourable and within the PEM for oppositely-charged particles and pore surfaces (indicated by white colour particles), or can be unfavourable within the SEM region for similarly-charged particles and pore surfaces (shown by red colour particles in different figures). DLVO energy plots in this study show considerable repulsive forces at close distances between particles and pore surfaces under unfavourable conditions which make deposition in PEM unlikely.

3.5. Particles transport equations and selected parameters

To simulate particles transport, different terms including hydrodynamic ($\boldsymbol{F}^H$), gravitational $\left(\boldsymbol{F}_P^G = \rho_P V_P g\left(1-\frac{\rho}{\rho_P}\right)\right)$, particle-surface DLVO ($\boldsymbol{F}_{P-S}^{DLVO}$) and particle-particle DLVO ($\boldsymbol{F}_{P-P}^{DLVO}$ forces are considered [24,34–36,38].

$$\boldsymbol{F}_{P-S}^{DLVO} = 4\pi\varepsilon_0\varepsilon_r\zeta_P\zeta_S\kappa R_P\left(\frac{exp(-\kappa h)}{1+exp(-\kappa h)} - \frac{(\zeta_P-\zeta_S)^2}{2\zeta_P\zeta_S}\frac{exp(-2\kappa h)}{1-exp(-2\kappa h)}\right) + \frac{H_a R_P}{6h^2} \tag{12}$$

$$\boldsymbol{F}_{P_i-P_j}^{DLVO} = 32\pi\varepsilon_{0\varepsilon_r}\kappa R_P\left(\frac{K_B T}{Ze}\right)^2 tanh\left(\frac{Ze\zeta_i}{4KT}\right)tanh\left(\frac{Ze\zeta_j}{4KT}\right)exp(-\kappa h) + \frac{32}{3}H_a D_{P_i-P_j}\frac{R_{P_i}^3 R_{P_j}^3}{\left(\left(\left(D_{P_i-P_j}+R_{P_i}\right)^2 - R_{P_j}^2\right)\left(\left(D_{P_i-P_j}-R_{P_j}\right)^2 - R_{P_i}^2\right)\right)^2} \tag{13}$$

All forces and torques (T_p) exerted on each particle are integrated using Eqs. (14) and (15) (i.e., equations of motion) to calculate each particle's translational and angular velocities ($\boldsymbol{U}_{Cp}$, $\boldsymbol{\omega}_p$). The new position ($\boldsymbol{R_P}$) is calculated using Eq. (16).

$$M_P\frac{d\boldsymbol{U}_{C_P}}{dt} = \boldsymbol{F}_P^H + \boldsymbol{F}_P^G + \boldsymbol{F}_{P-P}^{DLVO} + \boldsymbol{F}_{P-S}^{DLVO} \tag{14}$$

$$I_P.\dot{\boldsymbol{\omega}}_P = \boldsymbol{T}_P \tag{15}$$

$$\frac{d\boldsymbol{R_P}}{dt} = \boldsymbol{U}_{C_P} \tag{16}$$

In the above equations, $\kappa = (2\times10^3 N_A e^2 IS/\varepsilon_0\varepsilon_r K_B T)^{1/2}$ [m] is the reciprocal Debye length of a monovalent electrolyte, and M_P [Kg], I_P [Kg.m^2], V_P [m^3], Dij [m], and h [m] are mass, moment of inertia, volume, centre to centre distance, and surface separation distance of particles, respectively. The values of other parameters which remain constant during each simulation are given in Table 1.

To improve our understanding of how coupled effects of particles size, solution IS, particles and pore surface zeta potential, and average flow velocity can affect particles transport and retention mechanisms, three different values for each parameter are selected which are provided in Table 1. Parameter combinations resulted in a total of 162 different simulations representing both favourable and unfavourable conditions.

3.6. Rolling of colloids on the pore surface

Under unfavourable deposition conditions, when a particle reaches surface secondary minimum distance, a contact radius, $I_x = (F_r R_P/4K)^{1/3}$, is considered on the particle where F_r is sum of the resisting forces, and $K = 4.014\times10^9$ Nm^{-2} is the composite Young's modulus [14]. The comparison between applied hydrodynamic and resisting torques, calculated around each contact edge of the particle, determines whether the deposited particle can roll over the surface or remain immobile.

4. Geometry and boundary conditions

A 200 μm × 50 μm constricted pore shape with a 20 μm wide throat size is simulated using a 400 × 100 LBM rectangular grid. As boundary conditions, a no slip boundary is applied at the top and bottom sinusoidal surfaces of the pore using a curve boundary bounce back scheme [40]. Since a curved line does not fit into the lattice nodes, we have used this boundary condition which is based on both bounce back and spatial interpolation of the boundary position. The inlet parabolic velocity profile and the outlet pressure boundary are implemented using Zou and He method [41]. These conditions are chosen to obtain a desired steady-state average flow velocities, U, across the pore. When the flow reaches the steady state, particles enter the pore one by one and at random heights with constant rates. Injection rates are set so that the surface area of the entering particles with different sizes are equal per pore volume, PV, of solution injection. For example, when the bulk velocity is 10 m/d, these rates are equal to 100, 36, and 9 particles per second for 3, 5, and 10 μm particles, respectively.

Table 1
Constant and variable model parameters used in the simulations.

Constant parameters	Value
Fluid density, ρ	1000 [Kg/m^3]
Particle density, ρ_P	1055 [Kg/m^3]
Boltzmann constant, K_B	1.38×10^{-23} [J/K]
Electron charge, e	1.6×10^{-19} [C]
Vacuum permittivity, ε_0	8.85×10^{-12} [C^2/Jm]
Media dielectric constant, ε_r	78.54
Hamaker constant, H_a	1.5×10^{-21} [J]
Ion valence, Z	1
Avogadro's number, N_A	6.02×10^{23}
Temperature, T	298 [K]
Variable parameters	**Value**
Particle radius, R_P	1.5, 2.5, 5 [μm]
Solution Ionic strength, IS	0.001, 0.05, 0.3 [M]
Mean flow velocity, U	1, 5, 10 [m/d]
Particles and pore surface zeta potential, ζ	±17.5, ±45.56, ±60 [mV]

5. Results and discussion

5.1. Ionic strength effect

In this section we provide a range of processes which can occur depending on IS of the solution. An increase in solution IS lowers the energy barrier and increases the SEM depth. This condition promotes attachment of the approaching colloids to the aggregates or to the pore surface, and may cause multilayer retention of particles through SEM interactions. The SEM interactions also provide agglomerates with resistance against hydrodynamic rupture which intends to fragment larger bodies into smaller ones [42–44]. Fig. 1a, and b show full pore clogging under high IS solutions of 0.3 M, and different flow velocities for both 3, and 5 μm particles. Under unfavourable conditions as IS decreases, a weaker SEM develops at larger separation distances which makes it possible for the hydrodynamic force to overcome the DLVO interactions. In this study, very low values of secondary energy minimum (e.g., below 1 KT) are related to low IS solutions of 0.001 M in which long-term association of colloids on the solid-water-interface and with other colloids was not observed, and colloid attachment and aggregation were rather reversible. Retention of particles in secondary minimum, and their detachment to the bulk flow has been often stated as a responsible mechanism for the observed deviation of attachment efficiency from theoretical predictions based on retention solely in the PEM [45–48].

Under low IS of 0.001 M and favourable deposition conditions, pore clogging is unlikely (except for large size particles of 10 μm). Scattered attached particles prohibit further contact of the approaching particles with a fraction of the surface behind them called the shadow zone [49]. Our simulations have shown that the extent of the shadow zone depends highly on IS. As shown in Fig. 1c, under low IS solutions of 0.001 M, a considerable space is created between attached colloids on the surface. The contributing mechanism for development of the shadow zone is the presence of weak particle-particle interactions, enabling the hydrodynamic force to prevent retention of approaching particles to previously attached ones. However, under larger IS values and stronger DLVO interactions, the approaching particles can rotate over the attached particles and deposit next to them and no shadow zone is created, as shown in Fig. 1d. Ko and Elimelech (2000) showed that decreasing solution IS results in an increased shadow zone under a wide range of solution ionic strengths and flow velocities [49].

In this section mechanistic insights about particle-particle and particle-surface interactions were presented under various IS values. In the following sections, we will describe IS effect on particles aggregation, pore surface coverage, conductivity, and void fraction under favourable and unfavourable conditions, respectively.

5.2. Effect of IS on colloid transport and change of pore properties: favourable conditions

To explain the impact of IS on transport behaviour, we use Fig. 2a related to 5 μm particles, which presents the attachment behaviour by providing the applied conditions (including velocity, zeta potential, and IS), and the resulting behaviour (including clogging state, pore hydraulic conductivity, void fraction, coordination number, and pore surface coverage) under favourable deposition conditions. For each simulation, the stable values obtained after injecting several pore volumes of the solution are averaged over time.

Pore void fraction is considered as fraction of the pore space that is not covered by retained particles. As IS increases, single or multi-layered deposited particles reduce the pore space for freely moving agglomerates while creation of large agglomerates decreases conductivity. As shown in Fig. 2a, pore void fraction and conductivity in low IS solutions of 0.001 M, for which particles generally transport individually or in small size agglomerates, reach higher stable values in comparison with their values in 0.05 M solutions.

Particle agglomeration is analysed using coordination number which shows the number of connections among particles present in each agglomerate. Fig. 2a shows that by increasing solution IS from 0.001 M to 0.05 M, the average coordination number increases. The increased number of connections among particles shows tendency of particles to create rounded shape agglomerates [21].

Surface coverage is defined as fraction of the grain surface covered by deposited particles. It is increased with IS since the SEM depth and

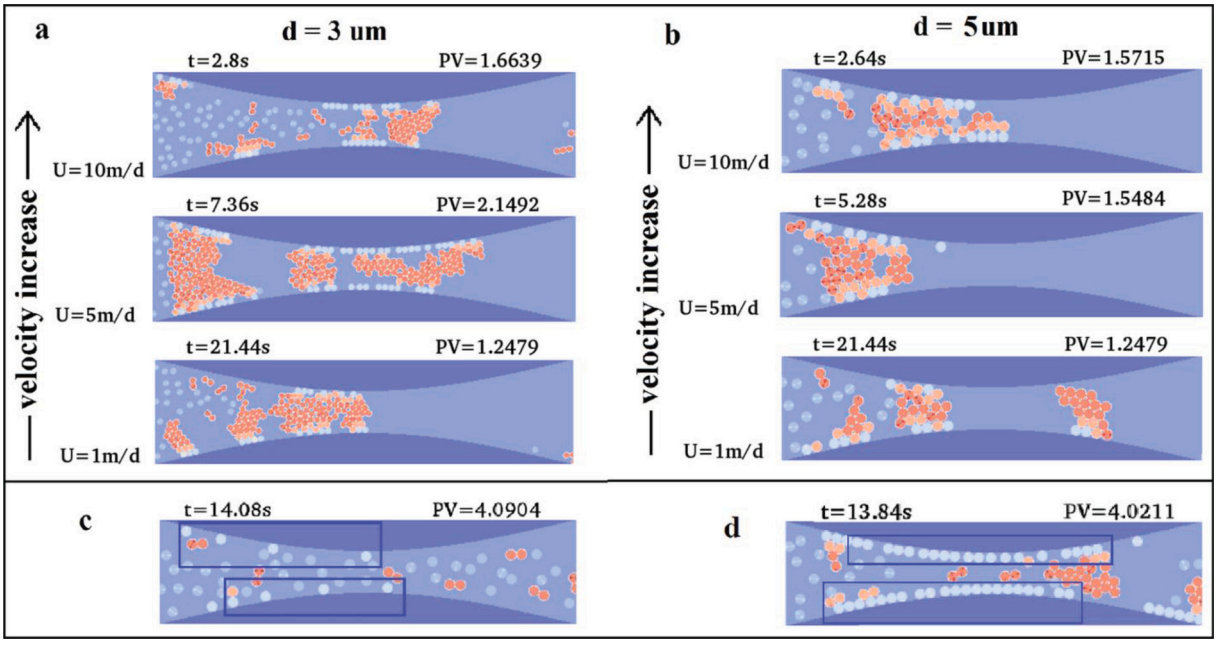

Fig. 1. Ionic strength effect on particles retention mechanisms. **(a, b)** In high IS solutions, pore clogging takes place for various particle sizes and velocities (IS = 0.3 M, ζ = 60 mV, favourable deposition conditions). **(a)** d_p=3 μm, **(b)** d_p=5 μm. **(c)** Low IS solutions enhances development of the shadow zone behind attached particles (d_p=5 μm, IS = 0.001 M, ζ = 17.5 mV, U = 5 m/d, favourable deposition conditions). **(d)** Attached particles make a compact surface layer under intermediate IS solutions (d_p = 5 μm, IS = 0.05 M, ζ = 60 mV, U = 5 m/d).

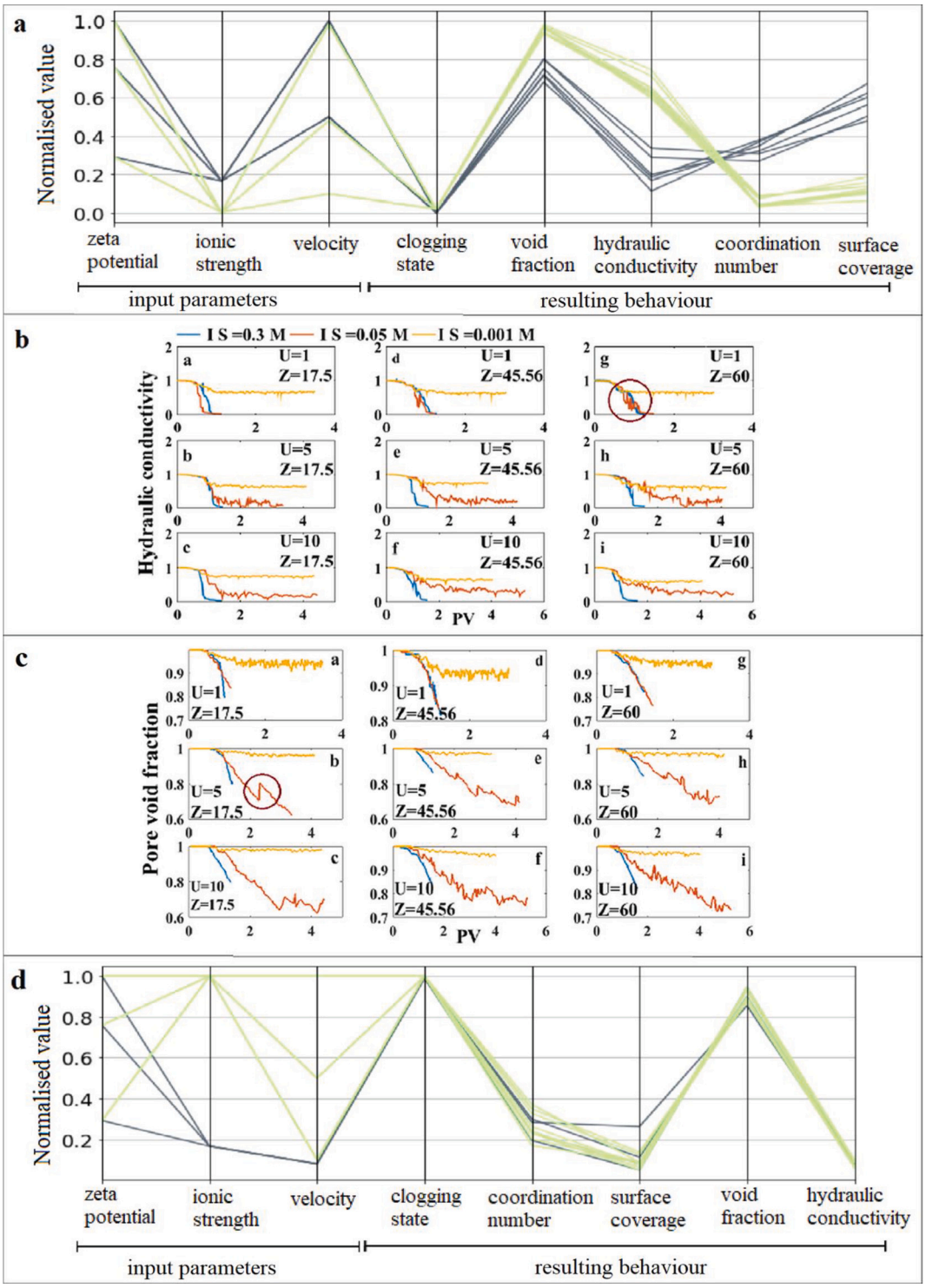

Fig. 2. The IS effects on transport properties under favourable deposition conditions. **(a)** Visualization of transport properties for unclogged pores with respect to IS under favourable deposition conditions ($d_p = 5$ μm). Green and gray lines are related to IS values of 0.001 M and 0.05 M, respectively. The first three axes show input parameters including zeta potential, ionic strength, and flow velocity. Other axes show the resulting behaviour including state of clogging (zero value indicates an unclogged pore), void fraction, hydraulic conductivity, coordination number, and pore surface coverage. Combination of input parameters are found by following each line on the first three axes. To make clearer graphs, each property is normalized by its maximum attainable value. The coordination numbers are normalized by the value of 6 since for circular shape colloids, each particle can be surrounded by a maximum of 6 particles. **(b)** Change of pore conductivity, and **(c)** pore void fraction with injected pore volumes at different IS solutions. Each small plot shows the simulations with the same zeta potential, Z [mV], and flow velocity, U [m/d], among which the IS is different. The blue, red and yellow graphs are related to IS values of 0.3 M, 0.05 M and 0.001 M, respectively. The fluctuations marked by red circles on these graphs are related to remobilization and breakup of agglomerates. **(d)** Visualization of transport properties for clogged pores (clogging state = 1) with respect to IS under favourable deposition conditions ($d_p = 5$ μm). Green and gray lines are related to IS values of 0.05 M and 0.3 M, respectively. (For interpretation of the references to colour in this figure legend, the reader is referred to the web version of this article.)

the tendency of particles for attachment on the surface increases [48,50]. Moreover, increase of solution IS creates large net-like agglomerates which their outermost particles can meet the pore surface while moving through the pore. Subsequently, the surface coverage increases. Ko and Elimelech (2000) showed that the rate of blocking and the maximum achievable surface coverage are determined by an interplay between fluid flow, particle size, and solution IS [49]. Our results show that both the higher tendency of particles for attachment on the surface, and the smaller developed shadow zones behind attached particles in high or intermediate IS solutions result in higher surface coverage (shown by gray lines in Fig. 2a). As previously discussed in Section 5.1, under an intermediate IS solution of 0.05 M, colloids tend to attach next to each other to form a compact surface layer resulting in high surface coverage values.

Fig. 2b and c shows the transient evolution of pore void fraction and hydraulic conductivity over time with respect to IS. The red and yellow graphs of Fig. 2b show that hydraulic conductivity can approach stable values, except for the simulations in which the pore clogs and conductivity reaches zero. However, the properties such as pore surface coverage or void fraction show a decreasing trend and may not reach stable values (shown by the red graphs in Fig. 2c, plots (b, e, h, i)). This is because these properties are based on arithmetic addition or subtraction of each particle local contribution, whereas the least conductive constriction inside the pore created by large agglomerates determines conductivity for the whole system. The fluctuating behaviour of the graphs, as marked by the red circles in Fig. 2b and c, are related to remobilization and breakup of agglomerates which causes fluctuations of the flow field, pore conductivity, and void fraction.

Fig. 2d presents the applied conditions and the attachment behaviour for a subset of simulations of 5 μm particles which ended up with pore clogging (clogging state = 1) under favourable deposition conditions. These include all 0.3 M solutions where creation of large agglomerates promotes pore clogging, as well as 0.05 M solutions under low flow velocity of 1 m/d where hydrodynamic forces cannot overcome SEM interactions among particles.

When pore clogging takes place, particles cannot reach downstream of the clogging location, and anticipations about decrease of void fraction or increase of pore surface coverage by increasing IS may not be fulfilled. For example, Fig. 2d shows that in 0.3 M solutions, surface coverage is relatively low for clogged pores with approximately zero conductivity. However, large convergent values of void fraction and low convergent values of surface coverage admit that there are enough pore surface and void space available inside the pore that are inaccessible for particles.

5.3. *Effects of IS on colloid transport and change of pore properties: unfavourable conditions*

Under unfavourable conditions, particle retention can happen at SEM distance and particles can roll over the pore surface, remain immobile on it, or detach to the bulk flow. These possibilities are due to the weaker SEM interactions between particles and the pore surface in comparison with primary minimum interactions under favourable conditions, and can be considered as the reason for different behaviour of particles under favourable and unfavourable conditions [12].

Fig. 3a compares simulations using 3 μm particles under

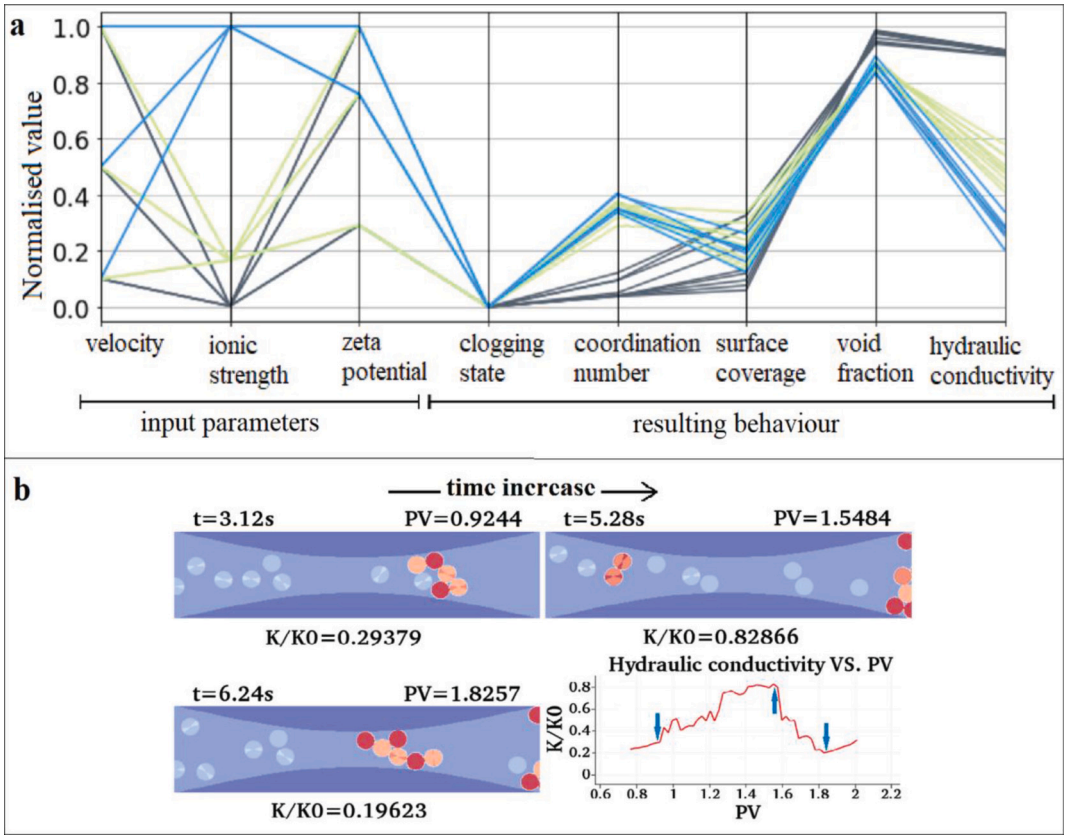

Fig. 3. The IS effects on transport properties under unfavourable deposition conditions. **(a)** Visualization of transport properties for unclogged pores including aggregates connectivity, pore surface coverage, pore void fraction, and hydraulic conductivity with respect to IS under unfavourable deposition conditions (d_p = 3 μm). The gray, green, and blue lines are related to IS values of 0.001 M, 0.05 M, and 0.3 M, respectively. Combination of input parameters can be found by following each line on the first three axes. **(b)** Clogging and re-opening of the pore due to rolling of aggregates on the pore surface which may cause conductivity fluctuations (d_p = 10 μm, IS = 0.05 M, ζ = 45.56 mV, U = 5 m/d). (For interpretation of the references to colour in this figure legend, the reader is referred to the web version of this article.)

unfavourable deposition conditions. This figure shows that low IS solutions of 0.001 M result in the lowest aggregate coordination numbers due to development of shallow SEM zones where hydrodynamic forces can detach the agglomerated particles. However, the coverage related to 0.001 M solutions in our unfavourable simulations showed a wide range among all observed values. These observations are due to the combined effects of IS and flow velocity which can affect particles retention and pore surface coverage. Detailed information can be found on Supplementary information, Fig. S2(a).

In Fig. 3a the highest pore void fraction and hydraulic conductivity are related to IS of 0.001 M due to less tendency of the particles for attachment on the surface or creating agglomerates. Pore conductivity is highly dependent on development of large size agglomerates, which are able to effectively reduce the pore size and to generate higher pressure drops across the pore. Pore conductivity and void fraction fluctuations, as the ones discussed under favourable conditions in Fig. 2b and c, can also be observed under unfavourable conditions. For example, Fig. 3b shows clogging of the pore by an agglomerate and its subsequent re-opening as the pore structure diverges due to rolling of 10 μm particles on the surface which results in conductivity fluctuations. We should note that fluctuations of conductivity under favourable and unfavourable deposition conditions can be attributed to different mechanisms. Under favourable deposition conditions, fluctuations are related often to remobilization or detachment of agglomerated particles from strongly deposited particles on the surface. Under unfavourable deposition conditions, agglomerates tend to clog the pore within the convergent section of the pore, however, the ability of the particles to roll on the surface helps them pass the pore throat and move into the divergent section. This process causes re-opening of the pore, so conductivity increases (Fig. 3b). Rolling of particles on the pore surface hinders strong clogging of the pore and increases pore conductivity. Few exceptions from this trend, e.g., simulations with high IS value of 0.3 M and low zeta potential of 17.5 mV, will be discussed in Section 5.5. These observations agree with the experimental observations of Kuznar and Elimelech who showed particles trapped within the secondary energy minimum moved downstream along the collector surface to deposit near the rear of spherical collectors [48]. Information on average coordination number of particles, surface coverage, pore hydraulic conductivity and void fraction against the injected pore volume is included in Supplementary information, Fig. S2.

5.4. Colloid-grain surface interactions

Fig. 4(a, b) compares particle-particle and particle-surface DLVO interactions. Due to the relatively flat shape of the pore structure compared to the curved surface of the colloids, DLVO interactions between particles are weaker than the interactions between particles and the surface. As an agglomerate moves through the pore, some of its constituting particles can enter the SEM distance of the surface. Due to their stronger interactions with the surface, these particles are detached from the aggregate to deposit on the pore surface as shown by the blue box in Fig. 4c. This mechanism often takes place close to the throat location where the pore structure diverges.

5.5. Zeta potential effect

Zeta potential (ζ) indicates the magnitude of surface charge of particles and mainly affects adsorption at longer time scales. Zeta potential effects can be explained by DLVO theory and expresses the stability of the system in the presence of different forces acting close to the interfaces [51]. High zeta potential, either positive or negative, is generally required to ensure stability. Thus, systems with zeta potentials $>\pm 30$ mV are generally considered stable. A major factor that affects zeta potential is solution pH. IS, the concentration of any additives, and temperature can also alter this parameter [52,53].

Under favourable deposition conditions, i.e., unlike-charged particles and pore surfaces, particle-surface interactions are activated at farther distances between charged surfaces as the magnitude of zeta potential increases. However, like-charged particles and pore surfaces make the surface deposition and colloid aggregation conditions unfavourable in which weaker DLVO interactions are expected at SEM distance as zeta potential increases. Therefore, stronger attractive SEM interactions are expected under lower zeta potential values among like-charged particles, which may result in higher coordination numbers of

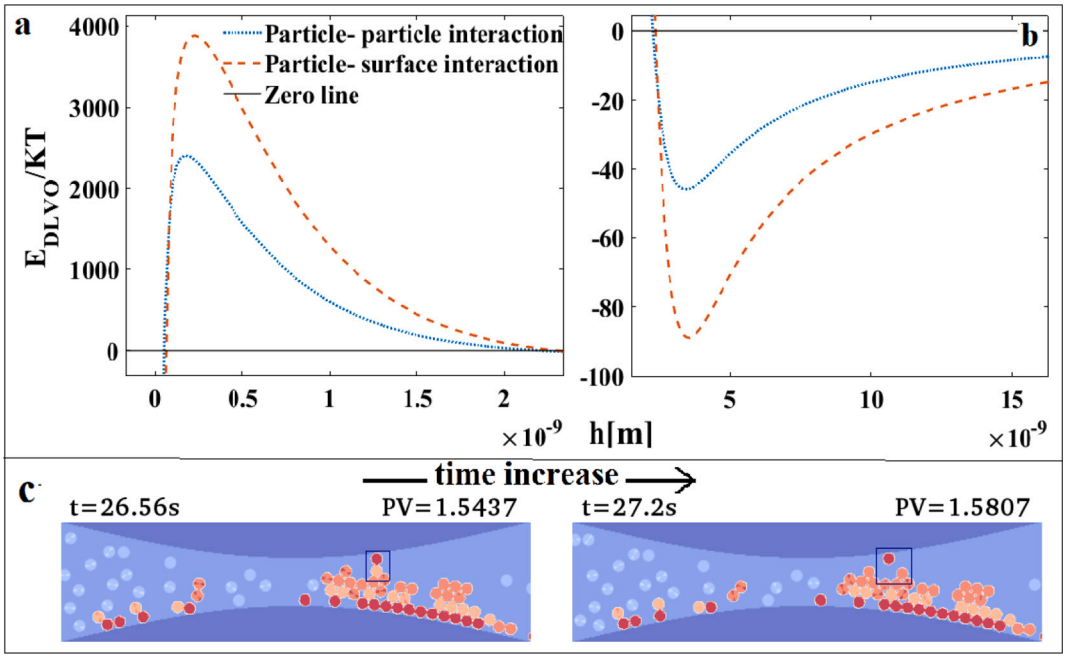

Fig. 4. Colloid-grain interactions. (a, b) Comparison of particle-particle and particle-surface DLVO interaction energy profiles ($d_p = 5$ μm, IS = 0.3 M, $\zeta = 45.56$ mV), **(a)** Development of energy barrier near the surface, **(b)** Development of SEM. **(c)** Separation of an agglomerate member to deposit on the pore surface ($d_p = 5$ μm, IS = 0.3 M, $\zeta = 60$ mV, $U = 1$ m/d).

aggregates, and lower pore void fraction and conductivity [10]. Dunphy Guzman et al. showed pH and surface potential dominate interactions among particles, while aggregate size generally increases as surface potential decreases [54]. Figs. 5 (a, b) show possibility of pore clogging in two situations where particles' zeta potential is decreased from 60 mV to 17.5 mV. Higher hydrodynamic forces are required to separate agglomerated particles with deep SEM interactions under lower zeta value of 17.5 mV, so the pore clogs (Fig. 5a). On the other hand, the reduced SEM depth under zeta potential value of 60 mV results in weaker DLVO interactions among particles, which can be overcome by hydrodynamic forces to prevent clogging (Fig. 5b).

As zeta potential values selected in this study are relatively close to each other, especially $\zeta = 45.56$ mV and $\zeta = 60$ mV, the expected changing trends for particles coordination number and pore properties with respect to zeta potential are not very obvious. As an example, simulation outcomes are shown in Fig. 5c for 5 μm particles under favourable deposition conditions. It is clear that as zeta potential changes, pore properties do not show a definite trend as multiple processes are involved. The same observations were also reported by other researchers. Lu and Gao mentioned zeta potential as one of the many indications affecting physical stability [52]. However, they mentioned it is sometimes not a directly relevant parameter for assessing stability when the difference of zeta potentials among various solutions is small. Moreover, Roland et al. did not observe any correlation between zeta potential (in the range of −43.1 to −50.2 mV) and the overall stability, while the most visually stable solutions in their case exhibited the lowest zeta potential [55]. Detailed sensitivity analysis of different parameters in our study showed that in the selected range of the parameters, IS effect dominates zeta potential effect. In the following, we discuss some important effects of zeta potential on particles behaviour.

Commonly, like-charged surfaces tend to repel each other; however, it is the combined effect of particle size, IS, and zeta potential which determines the ultimate interaction energy profiles. Fig. 5 (d, e) shows DLVO interaction energy profiles of 3 μm particles in high IS solution of 0.3 M. Fig. 5d shows a typical unfavourable energy profile under zeta potential value of 45.56 mV in which particles cannot reach primary minimum distance. However, under zeta potential of 17.5 mV, the barrier decreases to negative values, and particles can strongly attach on the surface (Fig. 5e). The coupled effect of high IS and low zeta potential values resulted in strong attachment of particles on the surface, and

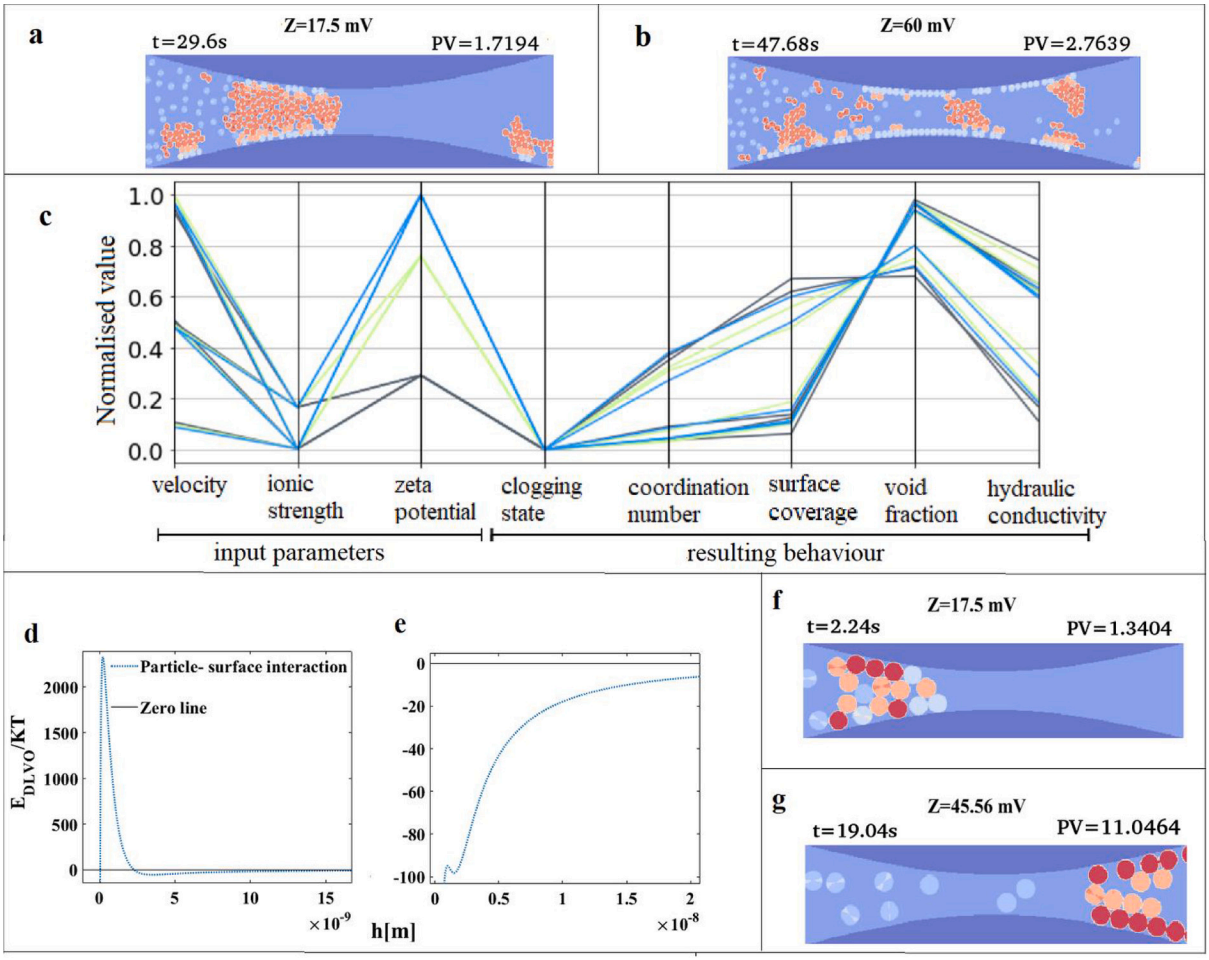

Fig. 5. Zeta potential effects on particles behaviour. (a) Possibility of pore clogging under low zeta potential values when considerable SEM interactions and low hydrodynamic forces are created ($dp = 3$ μm, IS = 0.05 M, $U = 1$ m/d, $\zeta = 17.5$ mV). **(b)** Hydrodynamic forces prevented clogging as they overcame weak SEM interactions among particles due to large zeta potential values ($dp = 3$ μm, IS = 0.05 M, $U = 1$ m/d, $\zeta = 60$ mV). **(c)** Sensitivity analysis showing change of aggregates connectivity, pore surface coverage, pore void fraction, and hydraulic conductivity for unclogged pores with respect to zeta potential under favourable deposition conditions ($d_p = 5$ μm). The gray, green, and blue lines are related to zeta potential values of 17.5, 45.56, and 60 mV, respectively. Combination of input parameters can be found by following each line on the first three axes. **(d, e)** Particle-surface DLVO interaction energy profiles under different zeta potential values ($dp = 3$ μm, IS = 0.3 M), **(d)** $\zeta = 45.56$ mV, **(e)** $\zeta = 17.5$ mV. **(f)** Low zeta potential in combination with high IS solution resulted in strong attachment of particles on the like-charged pore surface ($dp = 10$ μm, IS = 0.3 M, $U = 10$ m/d, $\zeta = 17.5$ mV). **(g)** Increase of zeta potential from 17.5 mV to 45.56 mV resulted in deposition of particles in the secondary minimum distance of the surface ($dp = 10$ μm, IS = 0.3 M, $U = 10$ m/d, $\zeta = 45.56$ mV, unfavourable deposition conditions). (For interpretation of the references to colour in this figure legend, the reader is referred to the web version of this article.)

subsequent pore clogging was observed for all particle sizes and flow velocities in our simulations although particles and the pore surface were similarly charged. Fig. 5f shows this condition for 10 μm particles where attached particles in primary distance of the surface have clogged the pore after injecting 1.3 PV solution. The same particles are shown in Fig. 5g under the same solution IS, but increased zeta potential of 45.56 mV. This increase of zeta value resulted in unfavourable deposition condition where particles are trapped at SEM distance and they can roll over the surface toward the outlet. The graphs showing how transport properties change against injected PV with respect to zeta potential under both favourable and unfavourable conditions, and detailed explanation about its effect on surface coverage are provided in Supplementary information, Figs. S3 and S4.

6. Summary and conclusions

A coupled numerical scheme using Lattice Boltzmann and Smoothed Profile methods was developed to simulate transport of colloids and aggregates in a single constricted pore. This method enabled a detail description of hydrodynamic, particle-surface and particle-particle interactions, their effects on transport of bulk and deposited particles, altering flow field and the pore shape. Formation, restructuring, and breakup of agglomerates, together with their effects on transport and retention processes were explored. The results provided valuable information on the underlying mechanisms of colloid transport and retention in porous media, and thus to ascertain mechanisms responsible for the observed behaviour at larger, macroscopic, scale and column experiments. In this study we found that:

- In comparison with zeta potential, IS had greater impacts on determining particles behaviour.
- The increase of IS resulted in greater interactions among particles, creation of larger agglomerates, decrease of pore void fraction and hydraulic conductivity, and a higher probability of pore clogging which agree with DLVO theory. However, there may be deviations from these trends that are explained by the complex interactions among charged surfaces and the combined effects of other parameters such as spatial-dependent hydrodynamic forces.
- Strong attachment of particles on the grain surface under favourable deposition conditions resulted in decrease of permeability toward complete pore clogging. However, under unfavourable deposition conditions rolling of particles on the grain surface prevented clogging.
- Pore clogging and the subsequent re-opening of the pore caused fluctuations in conductivity and void fraction. Under favourable deposition conditions, pore re-opening was often attributed to detachment of agglomerated particles from each other. However, under unfavourable conditions, it was attributed to rolling of the particles on the surface toward the divergent section of the pore even if the agglomerated particles were not detached from each other.
- Low zeta potential in combination with high IS solution resulted in attachment of particles on like-charged pore surfaces.
- The results obtained from a large number of simulations can help to understand the links between different transport and retention mechanisms needed to make reliable predictions in real situations. Furthermore, the results can be used to derive correlations for parameters such as retention/release rate coefficients in porous media. Such information provides underlying pore-scale evidences to explain observations made at larger scales such as column experiments where often pore-scale information is challenging to be obtained to support the interpretation of colloid breakthrough curves. While we used a simple constricted pore geometry due to the required computational time needed for all simulations, particularly in the presence of many particles inside the pore, future studies using more complex pore shapes and several interconnected pores can provide accurate sample-specific behaviours.

Author statement

All authors confirm that this paper has not been submitted to any other journals. It should be mentioned that all of authors agree to submit this manuscript to Colloid and Interface Science Communications. They also confirmed that this manuscript is their original work.

Declaration of Competing Interest

The authors have no conflict of interest to declare.

Appendix A. Supplementary information

Supplementary information to this article can be found online at https://doi.org/10.1016/j.colcom.2021.100389.

References

[1] J.F. Schijven, S.M. Hassanizadeh, Removal of viruses by soil passa0067e: overview of modeling, processes, and parameters, Crit. Rev. Environ. Sci. Technol. 30 (1) (2000 Jan 1) 49–127.
[2] M. Seidel, L. Jurzik, I. Brettar, M.G. Höfle, C. Griebler, Microbial and viral pathogens in freshwater: current research aspects studied in Germany, Environ. Earth Sci. 75 (20) (2016 Oct 1) 1384.
[3] M. Verani, I. Federigi, G. Donzelli, L. Cioni, A. Carducci, Human adenoviruses as waterborne index pathogens and their use for Quantitative Microbial Risk Assessment, Sci. Total Environ. 651 (2019 Feb 15) 1469–1475.
[4] J.F. Schijven, W. Hoogenboezem, M. Hassanizadeh, J.H. Peters, Modeling removal of bacteriophages MS2 and PRD1 by dune recharge at Castricum, Netherlands, Water Resour. Res. 35 (4) (1999 Apr) 1101–1111.
[5] J.F. Schijven, S.M. Hassanizadeh, R.H. de Bruin, Two-site kinetic modeling of bacteriophages transport through columns of saturated dune sand, J. Contam. Hydrol. 57 (3–4) (2002 Aug 1) 259–279.
[6] S. Sasidharan, S. Torkzaban, S.A. Bradford, P.J. Dillon, P.G. Cook, Coupled effects of hydrodynamic and solution chemistry on long-term nanoparticle transport and deposition in saturated porous media, Colloids Surf. A Physicochem. Eng. Asp. 457 (2014 Sep 5) 169–179.
[7] S. Sasidharan, S. Torkzaban, S.A. Bradford, P.G. Cook, V.V. Gupta, Temperature dependency of virus and nanoparticle transport and retention in saturated porous media, J. Contam. Hydrol. 196 (2017 Jan 1) 10–20.
[8] N. Sefrioui, A. Ahmadi, A. Omari, H. Bertin, Numerical simulation of retention and release of colloids in porous media at the pore scale, Colloids Surf. A Physicochem. Eng. Asp. 427 (2013 Jun 20) 33–40.
[9] N. Seetha, M.M. Kumar, S.M. Hassanizadeh, A. Raoof, Virus-sized colloid transport in a single pore: model development and sensitivity analysis, J. Contam. Hydrol. 164 (2014 Aug 1) 163–180.
[10] H. Yang, M.T. Balhoff, Pore-network modeling of particle retention in porous media, AICHE J. 63 (7) (2017 Jul) 3118–3131.
[11] S. Faghihi, A. Keykhosravi, K. Shahbazi, Modeling of kinetic adsorption of natural surfactants on sandstone minerals: spotlight on accurate prediction and data evaluation, Colloid Interface Sci. Commun. 33 (2019 Nov 1) 100208.
[12] M.S. Kermani, S. Jafari, M. Rahnama, A. Raoof, Direct pore scale numerical simulation of colloid transport and retention. Part I: fluid flow velocity, colloid size, and pore structure effects, Adv. Water Resour. 144 (2020 Oct 1) 103694.
[13] N. Seetha, S. Majid Hassanizadeh, M.S. Mohan Kumar, A. Raoof, Correlation equations for average deposition rate coefficients of nanoparticles in a cylindrical pore, Water Resour. Res. 51 (10) (2015 Oct) 8034–8059.
[14] S. Torkzaban, S.A. Bradford, S.L. Walker, Resolving the coupled effects of hydrodynamics and DLVO forces on colloid attachment in porous media, Langmuir 23 (19) (2007 Sep 11) 9652–9660.
[15] S. Torkzaban, S.A. Bradford, J.L. Vanderzalm, B.M. Patterson, B. Harris, H. Prommer, Colloid release and clogging in porous media: effects of solution ionic strength and flow velocity, J. Contam. Hydrol. 181 (2015 Oct 1) 161–171.
[16] S.A. Bradford, S. Torkzaban, A. Shapiro, A theoretical analysis of colloid attachment and straining in chemically heterogeneous porous media, Langmuir 29 (23) (2013 Jun 11) 6944–6952.
[17] S.A. Bradford, Y. Wang, H. Kim, S. Torkzaban, J. Šimůnek, Modeling microorganism transport and survival in the subsurface, J. Environ. Qual. 43 (2) (2014 Mar) 421–440.
[18] C. Wang, A.D. Bobba, R. Attinti, C. Shen, V. Lazouskaya, L.P. Wang, Y. Jin, Retention and transport of silica nanoparticles in saturated porous media: effect of concentration and particle size, Environ. Sci. Technol. 46 (13) (2012 Jun 11) 7151–7158.
[19] E. Palacios, J. Cervini-Silva, Aggregation of authigenic, ferromagnetic-diamagnetic nano-FexSy, Colloid Interface Sci. Commun. 18 (2017 May 1) 5–8.
[20] A.J. Perez, J.E. Patino, M. Soos, V.L. Morales, Morphology of shear-induced colloidal aggregates in porous media: consequences for transport, deposition, and re-entrainment, Environ. Sci. Technol. 1 (2020 Apr).
[21] Z. Peng, E. Doroodchi, G. Evans, DEM simulation of aggregation of suspended nanoparticles, Powder Technol. 204 (1) (2010 Dec 10) 91–102.

[22] I. Chowdhury, S.L. Walker, S.E. Mylon, Aggregate morphology of nano-TiO 2: role of primary particle size, solution chemistry, and organic matter, Environ Sci Process Impacts 15 (1) (2013) 275–282.
[23] B.A. Legg, M. Zhu, L.R. Comolli, B. Gilbert, J.F. Banfield, Impacts of ionic strength on three-dimensional nanoparticle aggregate structure and consequences for environmental transport and deposition, Environ. Sci. Technol. 48 (23) (2014 Dec 2) 13703–13710.
[24] F. Chaumeil, M. Crapper, Using the DEM-CFD method to predict Brownian particle deposition in a constricted tube, Particuology 15 (2014 Aug 1) 94–106.
[25] K.M. Yao, M.T. Habibian, C.R. O'Melia, Water and waste water filtration. Concepts and applications, Environ. Sci. Technol. 5 (11) (1971 Nov 1) 1105–1112.
[26] N. Tufenkji, M. Elimelech, Deviation from the classical colloid filtration theory in the presence of repulsive DLVO interactions, Langmuir 20 (25) (2004 Dec 7) 10818–10828.
[27] N. Tufenkji, M. Elimelech, Breakdown of colloid filtration theory: role of the secondary energy minimum and surface charge heterogeneities, Langmuir 21 (3) (2005 Feb 1) 841–852.
[28] S. Jafari, R. Yamamoto, M. Rahnama, Lattice-Boltzmann method combined with smoothed-profile method for particulate suspensions, Phys. Rev. E 83 (2) (2011 Feb 9), 026702.
[29] E.J. Javaran, M. Rahnama, S. Jafari, Combining Lees–Edwards boundary conditions with smoothed profile-lattice Boltzmann methods to introduce shear into particle suspensions, Adv. Powder Technol. 24 (6) (2013 Nov 1) 1109–1118.
[30] Y. Nakayama, R. Yamamoto, Simulation method to resolve hydrodynamic interactions in colloidal dispersions, Phys. Rev. E 71 (3) (2005 Mar 25), 036707.
[31] S. Succi, The Lattice Boltzmann Equation: For Fluid Dynamics and Beyond, Oxford university Press, 2001 Jun 28.
[32] L. Luo, Lattice-gas Automata and Lattice Boltzmann Equations for Two-dimensional Hydrodynamics, Ph.D. thesis, Georgia Institute of Technology, 1993.
[33] S. Chen, G.D. Doolen, Lattice Boltzmann method for fluid flows, Annu. Rev. Fluid Mech. 30 (1) (1998 Jan) 329–364.
[34] B.V. Derjaguin, L. Landau, Theory of the stability of strongly charged lyophobic sols and of the adhesion of strongly charged particles in solutions of electrolytes, Acta Physicochim. U.S.S.R. 14 (1941) 633–662.
[35] E.J. Verwey, J.T. Overbeek, Theory of the Stability of Lyophobic Colloids, Elsevier, Amsterdam, 1948.
[36] R.T. Hogg, T.W. Healy, D.W. Fuerstenau, Mutual coagulation of colloidal dispersions, Trans. Faraday Soc. 62 (1966) 1638–1651.
[37] J.P. Minier, A General Introduction to Particle Deposition. In Particles in Wall-bounded Turbulent Flows: Deposition, Re-Suspension and Agglomeration, Springer, Cham, 2017, pp. 1–36.
[38] Qiu Q. Theoretical and Computational Study of Colloid Transport and Retention in Saturated Soil Porous Media (Doctoral dissertation, University of Delaware).
[39] H. Ma, J. Pedel, P. Fife, W.P. Johnson, Hemispheres-in-cell geometry to predict colloid deposition in porous media, Environ. Sci. Technol. 43 (22) (2009 Nov 15) 8573–8579.
[40] M.H. Bouzidi, M. Firdaouss, P. Lallemand, Momentum transfer of a Boltzmann-lattice fluid with boundaries, Phys. Fluids 13 (11) (2001 Nov) 3452–3459.
[41] Q. Zou, X. He, On pressure and velocity boundary conditions for the lattice Boltzmann BGK model, Phys. Fluids 9 (6) (1997 Jun) 1591–1598.
[42] S. Dukhin, C. Zhu, R.N. Dave, Q. Yu, Hydrodynamic fragmentation of nanoparticle aggregates at orthokinetic coagulation, Adv. Colloid Interf. Sci. 114 (2005 Jun 30) 119–131.
[43] D. Zhou, D. Wang, L. Cang, X. Hao, L. Chu, Transport and re-entrainment of soil colloids in saturated packed column: effects of pH and ionic strength, J. Soils Sediments 11 (3) (2011 Apr 1) 491–503.
[44] S. Torkzaban, S.A. Bradford, J.L. Vanderzalm, B.M. Patterson, B. Harris, H. Prommer, Colloid release and clogging in porous media: effects of solution ionic strength and flow velocity, J. Contam. Hydrol. 181 (2015 Oct 1) 161–171.
[45] M.W. Hahn, D. Abadzic, C.R. O'Melia, Aquasols: on the role of secondary minima, Environ. Sci. Technol. 38 (22) (2004 Nov 15) 5915–5924.
[46] C. Shen, B. Li, Y. Huang, Y. Jin, Kinetics of coupled primary-and secondary-minimum deposition of colloids under unfavorable chemical conditions, Environ. Sci. Technol. 41 (20) (2007 Oct 15) 6976–6982.
[47] C. Shen, Y. Huang, B. Li, Y. Jin, Predicting attachment efficiency of colloid deposition under unfavorable attachment conditions, Water Resour. Res. 1 (2010 Nov) 46(11).
[48] Z.A. Kuznar, M. Elimelech, Direct microscopic observation of particle deposition in porous media: role of the secondary energy minimum, Colloids Surf. A Physicochem. Eng. Asp. 294 (1–3) (2007 Feb 15) 156–162.
[49] C.H. Ko, M. Elimelech, The "shadow effect" in colloid transport and deposition dynamics in granular porous media: measurements and mechanisms, Environ. Sci. Technol. 34 (17) (2000 Sep 1) 3681–3689.
[50] J. Nocito-Gobel, J.E. Tobiason, Effects of ionic strength on colloid deposition and release, Colloids Surf. A Physicochem. Eng. Asp. 107 (1996 Feb 20) 223–231.
[51] H. Ohshima, The derjaguin–landau–verwey–overbeek (dlvo) theory of colloid stability, in: Electrical Phenomena at Interfaces and Biointerfaces: Fundamentals and Applications in Nano-, Bio-, and Environmental Sciences 27, 2012 Jan 25.
[52] G.W. Lu, P. Gao, Emulsions and micro emulsions for topical and transdermal drug delivery, in: Handbook of Non-invasive Drug Delivery Systems, William Andrew Publishing, 2010 Jan 1, pp. 59–94.
[53] S. Sharma, P. Shukla, A. Misra, P.R. Mishra, Interfacial and colloidal properties of emulsified systems: pharmaceutical and biological perspective, in: Colloid and Interface Science in Pharmaceutical Research and Development, Elsevier, 2014 Jan 1, pp. 149–172.
[54] K.A. Dunphy Guzman, M.P. Finnegan, J.F. Banfield, Influence of surface potential on aggregation and transport of titania nanoparticles, Environ. Sci. Technol. 40 (24) (2006 Dec 15) 7688–7693.
[55] I. Roland, G. Piel, L. Delattre, B. Evrard, Systematic characterization of oil-in-water emulsions for formulation design, Int. J. Pharm. 263 (1–2) (2003 Sep 16) 85–94.